CR-152024

FINITE ELEMENT STABILITY ANALYSIS FOR COUPLED ROTOR AND SUPPORT SYSTEMS

Part III of Final Report Under Contract NAS2-7613

Prepared for the Ames Directorate, USAAMRDL

at Ames Research Center, Moffett Field, California

by

K. H. Hohenemser

and

S. K. Yin

Department of Mechanical Engineering

Washington University
School of Engineering and Applied Science
St. Louis, Missouri 63130

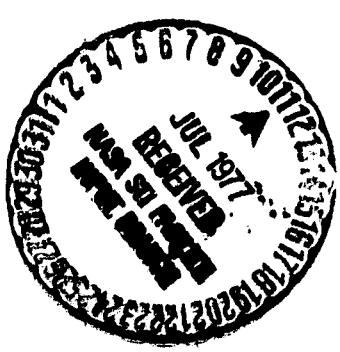

-June 1977-

FINITE ELEMENT STABILITY ANALYSIS FOR COUPLED ROTOR AND SUPPORT SYSTEMS

Part III of Final Report Under Contract NAS2-7613

Prepared for the Ames Directorate, USAAMRDL
at Ames Research Center, Moffett Field, California

by

K. H. Hohenemser

and

S. K. Yin

Department of Mechanical Engineering

Washington University
School of Engineering and Applied Science
St. Louis, Missouri 63130

-June 1977-

Finite Element Stability Analysis for Coupled Rotor and Support Systems

Part III of Final Report Under

Contract NAS2-7613

The conventional way of assessing the dynamic stability of coupled rotor airframe systems is to first determine a few undamped purely structural blade and airframe modes, to compute the aerodynamic reaction for each structural mode, and to consider an aeroelastic mode as a superposition of several structural modes, often of only two structural modes. The question then arises, how many structural modes are required for an adequate representation of an aeroelastic mode, a question that is not always easy to answer. The finite element analysis method investigated here avoids this difficulty and allows a direct computation of the aeroelastic modes. The characteristic equation of the total system is obtained by receptance or impedance matching at the interface between rotor and airframe. The method is studied for a case of hingeless rotor cyclic blade flap-bending motions in hovering coupled to rotor support rolling and pitching motions. Of the many aeroelastic rotor modes only two - the progressing first and the regressing second flap-bending modes - strongly couple with the rotor support modes and can become unstable for a range of rotor support stiffnesses.

Preface to Final Report under Contract NAS2-7613

Work under Contract NAS2-7613 started on July 1, 1973. The contract was originally awarded for a 3 year period.

Due to the slower than anticipated progress of the experimental work, not all research goals had been achieved by 30 June 1976. Since less than the anticipated cost for personnel and equipment had been spent, the research contract was extended by a year without increase in funding.

The research goals as stated in the contract were:

(a) Assess analytically the effects of fuselage motions on stability and random response. The problem is to develop an adequate but not overly complex flight dynamics analytical model and to study the effects of structural and electronic feedback, particularly for hingeless rotors.

(b) Study by computer and hardware experiments the feasibility of adequate perturbation models from non-linear trim conditions. The problem is to extract an adequate linear perturbation model for the purpose of stability and random motion studies. The extraction is to be performed on the basis of transient responses obtained either by computed time histories or by model tests.

(c) Extend the experimental methods to assess rotor wake-blade interactions by using a 4-bladed rotor model with the capability of progressing and regressing blade pitch excitation (cyclic pitch stirring), by using a 4-bladed rotor model with hub tilt stirring, and by testing rotor models in sinusoidal up or side flow.

Including the final report, 10 reports under Contract NAS2-7613 have been submitted. They are listed as P. 1 to P. 10 at the end of the Preface. P. 1 and P. 10 pertain to research goal (a). P. 2, P. 4, P. 6, P. 7, P. 8, P. 9, pertain to research goal (b). P. 3 and P. 5 pertain to research goal (c). The latter is not as yet complete since neither hub tilt stirring nor testing is sinusoidal up or side flow has been performed. While P. 10 describes only work done during FY 1977, P. 8 and P. 9 combine both FY 1977 work results and summaries of earlier results, so that the three parts of the Final Report can be read without recourse to the earlier reports. P. 8 includes much new material not available when the preceding Yearly Report P. 7 was written. The experimental data of P. 9 have all been obtained in FY 77.

So far 3 publications came out of the research under Contract NAS2-7613. They are listed as P. 11, P. 12, P. 13.

List of Reports and Papers under Contract NAS2-7613

P 1. Hohenemser, K. H. and Yin, S. K., "Methods Studies Toward Simplified Rotor-Body Dynamics", Part I of First Yearly Report under Contract NAS2-7613, June 1974.

P 2. Hohenemser, K. H. and Yin, S. K., "Computer Experiments in Preparation of System Identification from Transient Rotor Model Tests", Part II of First Yearly Report under Contract NAS2-7613, June 1974.

P 3. Hohenemser, K. H. and Crews, S. T., "Experiments with a Four-Bladed Cyclic Pitch Stirring Model Rotor", Part III of First Yearly Report under Contract NAS2-7613.

P 4. Hohenemser, K. H., Banerjee, D. and Yin, S. K., "Methods Studies on System Identification from Transient Rotor Tests", Part I of Second Yearly Report under Contract NAS2-7613, June 1975.

P 5. Hohenemser, K. H. and Crews, S. T., "Additional Experiments with a Four-Bladed Cyclic Pitch Stirring Model Rotor". Part II of Second Yearly Report under Contract NAS2-7613, June 1975.

P 6. Hohenemser, K. H., Banerjee, D. and Yin, S. K., "Rotor Dynamic State and Parameter Identification from Simulated Forward Flight Transients", Part I of Third Yearly Report under Contract NAS2-7613, June 1976.

P 7. Hohenemser, K. H. and Crews, S. T., "Rotor Dynamic State and Parameter Identification from Hovering Transients", Part II of Third Yearly Report under Contract NAS2-7613, June 1976.

P 8. Hohenemser, K. H. and Crews, S. T., "Unsteady Hovering Rotor Wake Parameters Identified from Dynamic Model Tests", Part I of Final Report under Contract NAS2-7613, June 1977.

P 9. Hohenemser, K. H. and Banerjee, D., "Application of System Identification to Analytic Rotor Modeling from Simulated and Wind Tunnel Dynamic Test Data", Part II of Final Report under Contract NAS2-7613, June 1977.

P 10. Hohenemser, K. H. and Yin, S. K., "Finite Element Stability Analysis for Coupled Rotor and Support Systems", Part III of Final Report under Contract NAS2-7613, June 1977.

P 11. Hohenemser, K. H. and Yin, S. K., "On the Use of First Order Rotor Dynamics in Multiblade Coordinates", 30th Annual National Forum of the American Helicopter Society, May 1974, Preprint 831.

P 12. Banerjee, D. and Hohenemser, K., "Optimum Data Utilization for Parameter Identification with Application to Lifting Rotors", Journal of Aircraft, Vol. 13, No. 12, December 1976, pp. 1014-1016.

P 13. Banerjee, D., Crews, S. T., Hohenemser, K. H. and Yin, S. K., Identification of State Variables and Dynamic Inflow from Rotor Model Dynamic Tests", Journal American Helicopter Society, Vol. 22, No. 2, April 1977.

Table of Contents

Nomenclature

EI	blade flap-bending stiffness
$\overline{EI}$	EI/EI_o flap-bending stiffness referred to root value
[E]	transfer matrix across massless blade element
[F]	transfer matrix across point mass
I	rotor support moment of inertia about rotor center
I_b	blade moment of inertia about rotor center
M	non-dimensional blade flap-bending moment (unit $\rho_o R^3 \Omega^2$)
N	number of finite elements per blade
P, Q	polynomials of λ
R	rotor radius
S	non-dimensional blade shear force (unit $\rho_o R^2 \Omega^2$)
T	non-dimensional blade centrifugal tension force (unit $\rho_o R^2 \Omega^2$)
X	state vector
a	blade airfoil lift slope
b	number of blades in rotor
c	non-dimensional blade chord (unit R)
c_i	aerodynamic damping coefficient for ith blade element
f_{Ai}	aerodynamic non-dimensional force at blade station i (unit $\rho_o R^2 \Omega^2$)
g_i	aerodynamic coefficient for blade pitch angle
l_i	non-dimensional length of blade element (unit R)
m_i	non-dimensional point mass at blade station i (unit $\rho_o R$)
p	$(T/q\ \overline{EI})^{1/2}$ blade tension force parameter

Nomenclature (cont')

q	$EI_o/\rho_o R^4\Omega^2$ non-dimensional blade root flap-bending stiffness
r_i	non-dimensional distance of blade station i from rotor center (unit R)
t	non-dimensional time (unit $1/\Omega$)
U_p, U_T	non-dimensional normal and tangential velocity at blade element (unit ΩR)
x	non-dimensional distance from outer end of blade element inboard (unit R)
y	non-dimensional blade deflection, positive up (unit R)
z	a single blade variable
θ	blade pitch angle, positive nose-up
$[\phi]$	transfer matrix
ψ_k	azimuth angle of kth blade
Ω	rotor angular speed
α	hub tilt angle
ξ	real part of coupled frequency (unit Ω)
λ	$\xi \pm i\omega$, non-dimensional complex valued frequency, (unit Ω)
ρ	non-dimensional air density (unit ρ_o/R^2)
ρ_c	blade mass per unit length at blade root
ω	circular frequency (unit Ω)

Subscripts

I, II	multiblade coordinates, forward and left respectively
i	value at ith blade element, beginning at blade tip
12, 13 ...	denotes elements of a determinant or matrix

Nomenclature (cont')

$1; \cdots N+1$	denotes values at blade tip and blade root
I, R	imagirary and real parts
M, α, θ	polynomials multiplied by M_{N+1}, α, θ
l, r	left, right of mass m_i

Superscripts

$\cdot$	time differentiation
$'$	length differentiation
-	truncated polynomials

Introduction

For the dynamic design of lifting or propeller rotors one usually begins by studying potential single blade dynamic instabilities. They can be caused by the effects of coupling between blade flap-bending, lag-bending, and torsion, by the periodicity of the aerodynamic stiffness and damping coefficients, or by unsteady aerodynamics phenomena. Even for stable single blade dynamics, potential instabilities can still exist, caused by the coupling of the blades with each other, with the rotor support or airframe, and with the rotor controls. A widely used approach to the problem of rotor dynamic stability, loads and vibrations is to first compute a few purely structural blade normal modes, using for example the methods of references 1 and 2, and then to consider the aeroelastic modes as truncated series of the structural normal modes. The truncation error is sensitive to the details of handling the aerodynamic loads, see for example references 3 and 4. The truncated normal structural mode expansion is either used as the basis of non-linear "global" computer programs as for example Rexor or MOSTAB, or it is used in linear eigenvalue programs as for example in reference 5, where two flapwise bending modes, two chordwise bending modes, one elastic torsion mode, and a few airframe and control modes are considered.

The problem with the undamped structural normal mode analysis is that in particular the low flap-bending aeroelastic modes are substantially affected by aerodynamics so that sizeable errors can be expected when only a few purely structural normal flap-bending modes are used. In a finite element stability analysis these errors are avoided and the aeroelastic modes are obtained directly. A finite element eigenvalue analysis results in a high order characteristic equation and requires a high precision computer program. The concept to be studied here is to perform a separate finite element eigenvalue analysis for the rotor and for the airframe, and then to couple both systems with the help of kinematic and equalibrium equations taken at the interface. A simple rotor and support representation is selected to gain some initial experience with the finite element stability analysis.

Modeling of Rotor and Support System

A schematic view of the rotor and support system used for the analysis is shown in Fig. 1. The blades are assumed rigid in chordwise bending and torsion, but flexible in flap-bending. They are rigidly connected to the hub so that the slope of the deflection line relative to the hub is constant and equal to the built-in coning angle. Since blade deflections and coning angle are small and only out-of-plane blade bending is considered, the built-in coning angle has no effect on rotor dynamics. The rotor shaft is assumed to be rigid and connected to a rigid housing that is supported by a focussing mount with focus on the

rotor center. Thus the hub is rigidly restrained against vertical and sidewise motions. The elastic restraints in pitch and roll of the hub are indicated in Fig. 1 by the horizontal springs attached to the shaft housing. There also is a gravitational restraint (pendulum effect). The restraining springs may have different stiffness in pitch or roll.

Fig. 2 shows the hub with a blade cross section in a position of angular deflection in pitch. It is assumed that the blades perform a uniform rotation about the vertical axis Z-Z. In actuality the rotational motion is non-uniform in a complex way depending on chordwise blade-bending and drive system dynamics. The vertical blade deflections are measured from the horizontal reference plane through the rotor center, indicated in Fig. 2 by X-X. Aerodynamic forces on the blades are produced by their vertical motions with respect to the reference plane (aerodynamic damping) and also by the blade pitch angle changes with respect to the reference plane, as seen in Fig. 2. It is assumed that the vertical blade motions and pitch angle changes do not produce a change in vertical inflow through the reference plane, an assumption approximately satisfied for the higher frequency regime that will be here of primary interest. Blade pitch controls are assumed to be rigid so that the blade pitch angle is equal to the hub tilting angle about the blade axis, indicated in Fig. 2 by $\alpha_I = \Theta_I$.

Blades with constant chord and uniform mass and flap-bending stiffness are assumed, though the method of analysis is suitable also for arbitrary blade planform and for non-uniform mass and stiffness distribution. The

uniform blade flap-bending stiffness extends to the rotor center. In actual hingeless rotor designs the hub is very stiff and the root section of the blade is more flexible then the rest of the blade. Extending the uniform blade flap-bending flexibility to the rotor center results, however, in first and second bending mode natural frequencies typical of actual hingeless rotors.

The analysis is performed in a non-dimensional way with length unit R, mass unit $\rho_o R$ and time unit $1/\Omega$. The force unit then becomes $\rho_o R^2\Omega^2$, the unit of angular inertia becomes $\rho_o R^3$, and the unit of bending stiffness becomes $\rho_o R^4\Omega^2$. For given mass and flap-bending distribution the rotor blades are described by the non-dimensional blade root bending stiffness q and by the blade Lock number γ. The rotor support is described by the ratio of blade moment of inertia over support moment of inertia, both taken about the rotor center, I_b/I, and further by the two non-dimensional support frequencies without blades ω_I and ω_{II}. Thus the rotor and support system is uniquely defined by 5 parameters: q, γ, I_b/I, ω_I, ω_{II}. The parameter $q^{-1/2}$ is proportional to the rotor angular speed Ω and can be used as rotor speed parameter. In the numerical examples $q^{-1/2} = 18$ is selected to simulate the dynamics of actual hingeless rotors. The remaining parameters are then varied within wide limits.

Method of Analysis

Reference 1 describes an analysis for determining the undamped structural single blade bending modes and frequencies with the help of blade element transfer matrices. The natural frequencies are obtained

by establishing through trial and error the zeros of the characteristic determinant, a method that is not feasible for unconservative systems. The following four steps are taken in extension of reference 1.

1. Aerodynamic terms are included in the blade transfer matrix.
2. Relations between blade root state variables are derived including a dynamid blade pitch feedback term.
3. Single blade polynomials are transformed into multiblade polynomials.
4. The total system characteristic equation is derived by receptance or impedance matching.

In a later section an intermediate step will be inserted between Steps 2 and 3 to reduce the order of the characteristic equation.

Blade Element Transfer Matrix

Fig. 3 shows a blade element between station i(outer end of element) and station i + 1 (inner end of element). The centrifugal force is assumed to act in the undeformed position of the blade and produces a bending moment $T_i y_i$. The moment M_i is thus fictitious and $M_i + T_i y_i$ is the actual bending moment acting on the outer end of the blade element. All quantities are non-dimensional with the units listed before. The inertia force $-\ddot{y}_i m_i = -\lambda^2 m_i y_i$ and the aerodynamic damping force $-\dot{y}\, c_i = -\lambda\, c_i y_i$ are added to the shear force at the point mass m_i. Also added is the aerodynamic force from dynamic blade pitch θ, expressed as $g_i\, \theta$. Since the blade is rigid in torsion, θ is constant along the radius. Dynamic pitch θ is caused by hub motions, see Fig. 2. Denoting

by l and r quantities to the left and right of the point mass m_i, we have

$$S_{il} = S_{ir} - (\lambda^2 m_i y_i + \lambda c_i y_i) + g_i \Theta \tag{1}$$

The change of the fictitious moment across the point mass is $-m_i r_i y_i$, since this incremental centrifugal force is assumed to be located in the undeformed blade position rather than at the mass m_i. Thus

$$M_{il} = M_{ir} - m_i r_i y_i \tag{2}$$

Over the length of the blade element l_i bending stiffness $\overline{EI}_q$ and centrifugal force T are constant. The deflection y is determined from the differential equation of beam bending

$$y'' \overline{EI}_q = Sx + (M + Ty) \tag{3}$$

where x is measured from the outer end of the blade element inboard. S and M are shear force and fictitious bending moment to the left of a point mass m_i. The slope $y'(x)$ is positive when opposite to y'_i shown in Fig. 1. The solution to Eq. (3) is

$$y(x) = y(0)\cosh(px) + (y'(0)/p)\sinh(px) \tag{4}$$
$$+ (M/T)[\cosh(px) - 1] + (S/T)[(1/p)\sinh(px) - x]$$

The derivative is:

$$y'(x) = y(0)\, p \sinh(px) + y'(0) \cosh(px)$$
$$+ (M/T)\, p \sinh(px) + S/T[\cosh(px) - 1] \tag{5}$$

where $p = (T/q\,\overline{EI})^{1/2}$ (6)

The fictitious bending moment is

$$M(x) = M + Sx \tag{7}$$

The shear force is constant

$$S(x) = S \tag{8}$$

Denoting the state vector by

$$X = \begin{bmatrix} S \\ M \\ y' \\ y \\ \Theta \end{bmatrix} \tag{9}$$

one can now write the change of the state vector along the blade element as a product of two matrices

$$X_{i+1} = [E]\,[F]\,X_i \tag{10}$$

The matrix [F] gives the change in state vector from the right side of the mass m_i to the left side and expresses Eqs. (1) and (2) together with the continuity relations $y_l' = y_r'$, $y_l = y_r$, $\Theta_l = \Theta_r$

$$[F] = \begin{bmatrix} 1 & 0 & 0 & -(\lambda^2 m_i + \lambda c_i) & g_i \\ 0 & 1 & 0 & -m_i r_i & 0 \\ 0 & 0 & 1 & 0 & 0 \\ 0 & 0 & 0 & 1 & 0 \\ 0 & 0 & 0 & 0 & 1 \end{bmatrix} \tag{11}$$

The matrix [E] gives the change in state vector from the left side of the mass m_i to the right side of the mass m_{i+1}. It expresses Eqs. (4) to (8) considering that $y'_i = -y'(0)$, $y'_{i+1} = -y'(l_i)$, $\Theta_{i+1} = \Theta_i$. The matrix [E] then is

$$[E] = \begin{bmatrix} 1 & 0 & 0 & 0 & 0 \\ l_i & 1 & 0 & 0 & 0 \\ E_{31} & E_{32} & E_{33} & E_{34} & 0 \\ E_{41} & E_{42} & E_{43} & E_{44} & 0 \\ 0 & 0 & 0 & 0 & 1 \end{bmatrix} \tag{12}$$

where

$$\begin{aligned} E_{31} &= -E_{42} = -(1/T_i)[\cosh\ (p_i l_i) - 1] \\ E_{32} &= -(1/T_i)\ p_i \sinh\ (p_i l_i) \\ E_{33} &= E_{44} = \cosh\ (p_i l_i) \\ E_{34} &= p_i \sinh\ (p_i l_i) \\ E_{41} &= (1/T_i)(1/p_i) \sinh\ (p_i l_i) \\ E_{43} &= -(1/p_i) \sinh\ (p_i l_i) \\ p_i &= (T_i/q\ \overline{EI}_i)^{1/2} \end{aligned} \tag{13}$$

In comparing these expressions with those given in reference 1 one should note that λ is defined differently leading to the opposite sign of λ^2 in Eq. (11). Furthermore the unit of circular frequency in reference 1 is $(EI_o/\rho_o R^4)^{1/2}$, while it is here Ω.

Denoting the matrix product $[E][F] \equiv [\phi]$, Eq. (10) can be written in the form

$$X_{i+1} = [\phi_i]X_i \tag{14}$$

For N masses one obtains by successive transfer matrix multiplication, beginning at the blade tip, for the root quantities the following relation

$$\begin{bmatrix} S_{N+1} \\ M_{N+1} \\ y'_{N+1} \\ y_{N+1} \end{bmatrix} = \begin{bmatrix} \phi_{11} & \phi_{12} & \phi_{13} & \phi_{14} \\ \phi_{21} & \phi_{22} & \phi_{23} & \phi_{24} \\ \phi_{31} & \phi_{32} & \phi_{33} & \phi_{34} \\ \phi_{41} & \phi_{42} & \phi_{43} & \phi_{44} \end{bmatrix} \begin{bmatrix} S_1 \\ M_1 \\ y'_1 \\ y_1 \end{bmatrix} + \begin{bmatrix} \phi_{15} \\ \phi_{25} \\ \phi_{35} \\ \phi_{45} \end{bmatrix} \Theta \tag{15}$$

All elements of $[\phi]$ are polynomials of λ. Eq. (15) completes step one. Before proceeding further, the aerodynamic coefficients c_i and g_i must be determined.

Aerodynamic Coefficients

As before, x is measured from the outer end of the blade element toward the rotor center. Non-dimensional tangential and normal flow velocities at the blade element u_T and u_P are, if dynamic inflow is ignored, and if u_P is averaged over l_i:

$$u_T = r_i - x \quad , \quad u_P = -(1/2)(\dot{y}_1 + \dot{y}_{i+1}) \tag{16}$$

The non-dimensional aerodynamic force acting on the blade element of length l_i is:

$$f_A = (1/2) \int_0^{l_i} \rho \, ac(\theta \, u_T^2 + u_p \, u_T)dx \tag{17}$$

Introducing the Lock number for a uniform blade which takes in our non-dimensional units the form $\gamma = 3 \rho \, ac$, and inserting Eq. (16) into Eq. (17):

$$f_A = (1/6)\gamma \int_0^{l_i} \{\theta \, (r_i - x)^2 - (1/2)(\dot{y}_i + \dot{y}_{i+1})(r_i - x)\}dx \tag{18}$$

Performing the integrations:

$$f_A = (1/6)\gamma \, \theta(r_i^2 \, l_i - r_i \, l_i^2 + l_i^3/3)$$

$$- (1/12)\gamma \, (\dot{y}_i + \dot{y}_{i+1})(r_i l_i - l_i^2/2) \tag{19}$$

One half of the first term is assumed to act at station i, the other half at station i+1. Of the second term the force with factor $\dot{y}_i$ is assumed to act at station i, the force with factor $\dot{y}_{i+1}$ at station i+1. With this assumed distribution of the aerodynamic forces the total aerodynamic force at station i is:

$$f_{Ai} = (1/12)\gamma \; [\theta(r_{i-1}^2 \, l_{i-1} - r_{i-1} \, l_{i-1}^2 + l_{i-1}^3/3$$

$$+ r_i^2 \, l_i - r_i \, l_i^2 + l_i^3 \, /3) - \dot{y}_i(r_{i-1} \, l_{i-1} - l_{i-1}^2/2$$

$$+ r_i \, l_i - l_i^2/2] \tag{20}$$

The factor of θ is equal to g_i, the factor of $\dot{y}_i$ is equal to c_i.

Blade Root Relations

Equation (15) relates the variables at the blade tip to those at the blade root. We need, however, a relation between blade root variables. Two variables at the tip are known, since shear force and bending moment are zero. The centrifugal force is also zero at the tip, thus the fictitious bending moment is zero. There is no vertical motion at the rotor center, so that

$$y_{N+1} = M_1 = S_1 = 0 \tag{21}$$

The two remaining tip variables y_1', y_1 will be expressed in blade root variables, as follows

Inserting Eq. (21) into Eq. (15) we have

$$\begin{bmatrix} S_{N+1} \\ M_{N+1} \end{bmatrix} = \begin{bmatrix} \phi_{13} & \phi_{14} \\ \phi_{23} & \phi_{24} \end{bmatrix} \begin{bmatrix} y_1' \\ y_1 \end{bmatrix} + \begin{bmatrix} \phi_{15} \\ \phi_{25} \end{bmatrix} \Theta \tag{22}$$

$$\begin{bmatrix} y_{N+1}' \\ 0 \end{bmatrix} = \begin{bmatrix} \phi_{33} & \phi_{34} \\ \phi_{43} & \phi_{44} \end{bmatrix} \begin{bmatrix} y_1' \\ y_1 \end{bmatrix} + \begin{bmatrix} \phi_{35} \\ \phi_{45} \end{bmatrix} \Theta \tag{23}$$

From Eq. (23):

$$\begin{bmatrix} y_1' \\ y_1 \end{bmatrix} = \begin{bmatrix} \phi_{33} & \phi_{34} \\ \phi_{43} & \phi_{44} \end{bmatrix}^{-1} \left(\begin{bmatrix} y_{N+1}' \\ 0 \end{bmatrix} - \begin{bmatrix} \phi_{35} \\ \phi_{45} \end{bmatrix} \Theta \right) \tag{24}$$

We now substitute Eq. (24) into Eq. (22):

$$\begin{bmatrix} S_{N+1} \\ M_{N+1} \end{bmatrix} = \begin{bmatrix} \phi_{13} & \phi_{14} \\ \phi_{23} & \phi_{24} \end{bmatrix} \begin{bmatrix} \phi_{33} & \phi_{34} \\ \phi_{43} & \phi_{44} \end{bmatrix}^{-1} \left(\begin{bmatrix} y'_{N+1} \\ 0 \end{bmatrix} - \begin{bmatrix} \phi_{35} \\ \phi_{45} \end{bmatrix} \theta \right) + \begin{bmatrix} \phi_{15} \\ \phi_{25} \end{bmatrix} \tag{25}$$

After performing the required manipulations, one obtains for the second equation

$$M_{N+1} P_M(\lambda) = y'_{N+1} P_\alpha(\lambda) + \theta P_\theta(\lambda)$$

where $P_M(\lambda) = \begin{vmatrix} \phi_{33} & \phi_{34} \\ \phi_{43} & \phi_{44} \end{vmatrix}$, $P_\alpha(\lambda) = \begin{vmatrix} \phi_{23} & \phi_{24} \\ \phi_{43} & \phi_{44} \end{vmatrix}$, $P_\theta(\lambda) = \begin{vmatrix} \phi_{23} & \phi_{33} & \phi_{43} \\ \phi_{24} & \phi_{34} & \phi_{44} \\ \phi_{25} & \phi_{35} & \phi_{45} \end{vmatrix}$

(26)

Equation (26) can only be used for a single blade characteristic equation, if the dynamic pitch angle θ is either zero or related to a root variable. For example a hinged blade without pitch-flap coupling, $M_{N+1} = \theta = 0$, gives as characteristic equation

$$P_\alpha(\lambda) = 0 \tag{27}$$

A hinged blade with a pitch-flap coupling defined by $\theta = k y'_{N+1}$, gives the characteristic equation

$$P_\alpha(\lambda) + k P_\theta(\lambda) = 0 \tag{28}$$

Finally a cantilever blade, where $y'_{N+1} = \Theta = 0$ gives the characteristic equation

$$P_M(\lambda) = 0$$

This completes step 2 of the analysis.

Multi Blade Transformations

The relations between single blade and multi blade coordinates are, when only cyclic terms are retained, see reference 6,

$$\begin{aligned} (y'_{N+1})_k &= \alpha_I \cos \psi_k + \alpha_{II} \sin \psi_k \\ \Theta_k &= \Theta_{II} \cos \psi_k - \Theta_I \sin \psi_k \\ (M_{N+1})_k &= M_I \cos \psi_k + M_{II} \sin \psi_k \end{aligned} \tag{30}$$

α_I, M_I, Θ_I refer respectively to nose down rotor tilting angle, nose down rotor moment on its support, and nose down cyclic pitch angle. α_{II}, M_I, Θ_{II} refer to left rotor tilting angle, left rotor moment on its support, and left cyclic pitch angle. Equations (30) are easily inverted.

For example

$$\alpha_I = (2/b) \sum_{k=1}^{b} (y'_{N+1})_k \cos \psi_k \tag{31}$$

with b the number of blades of the rotor. Eqs. (30) and (31) are valid for $b \geq 3$. Equation (26) is now transformed into relations between multiblade coordinates. The question is how to transform a polynomial of λ for a single blade coordinate into polynomials of λ for multiblade coordinates. Each factor of λ corresponds to a differentiation. Assume an arbitrary single blade variable z and its multiblade counterpart z_I, z_{II} related by

$$z = z_I \cos t + z_{II} \sin t \tag{32}$$

whereby the azimuth angle has been written in the form of the non-dimensional time t in which the time of one rotor revolution is equal to 2π. Differentiating Eq. (32) once:

$$\dot{z} = (\dot{z}_I + z_{II})\cos t + (-z_I + \dot{z}_{II})\sin t \tag{33}$$

Differentiating a second time:

$$\ddot{z} = (\ddot{z}_I - z_I + 2\,\dot{z}_{II})\cos t - (-2\dot{z}_I + \ddot{z}_{II} - z_{II})\sin t \tag{34}$$

Replacing the differential quotients by factors of λ Eqs. (33) and (34) read

$$\lambda z = (\lambda z_I + z_{II})\cos t + (-z_I + \lambda z_{II})\sin t \tag{35}$$

$$\lambda^2 z = (z_I(\lambda^2 - 1) + 2\lambda\, z_{II})\cos t + (-2\lambda\, z_I + z_{II}(\lambda^2-1))\sin t \tag{36}$$

Let us replace in the polynomial on the left hand side λ by $(\lambda+Y)$ and let us then form a matrix that has as diagonals the real parts of the left hand side polynomial and as off diagonal terms the plus and minus

imaginary parts of the polynomial, plus being used for the first row. For Eq. (35) this matrix reads

$$\begin{bmatrix} \lambda & 1 \\ -1 & \lambda \end{bmatrix}$$

For Eq. (36) this matrix reads, since $(\lambda + i)^2 = \lambda^2 - 1 + 2i\,\lambda$

$$\begin{bmatrix} \lambda^2 - 1 & 2\lambda \\ -2\lambda & \lambda^2 - 1 \end{bmatrix}$$

Post multiplying these matrices by the column $[z_I/z_{II}]$ one obtains

$$\begin{bmatrix} \lambda & 1 \\ -1 & \lambda \end{bmatrix} \begin{bmatrix} z_I \\ z_{II} \end{bmatrix} = \begin{bmatrix} \lambda\, z_I \\ -z_I \end{bmatrix} + \begin{bmatrix} z_{II} \\ \lambda z_{II} \end{bmatrix} \tag{37}$$

$$\begin{bmatrix} \lambda^2 - 1 & 2\lambda \\ -2\lambda & \lambda^2 - 1 \end{bmatrix} \begin{bmatrix} z_I \\ z_{II} \end{bmatrix} = \begin{bmatrix} z_I\,(\lambda^2 - 1) \\ -z_I\ 2\lambda \end{bmatrix} + \begin{bmatrix} z_{II}\ 2\lambda \\ z_{II}(\lambda^2 - 1) \end{bmatrix} \tag{38}$$

Equations (37) and (38) yield the factors of cos t and sin t in Eqs. (35) and (36). In general, if a single blade coordinate z is multiplied by a polynomial $P(\lambda)$ as in Eq. (26), one obtains the multiblade expressions by splitting the polynomial $P(\lambda + i)$ in real and imaginary parts: $P(\lambda + i) = P_R(\lambda) + i\,P_I(\lambda)$ and by writing

$$\begin{bmatrix} P_R(\lambda) & P_I(\lambda) \\ -P_I(\lambda) & P_R(\lambda) \end{bmatrix} \begin{bmatrix} z_I \\ z_{II} \end{bmatrix} \tag{39}$$

To apply this rule, we write Eq. (26) as

$$M_{N+1}\, P_M(\lambda+i) = y'_{N+1}\, P_\alpha(\lambda+i) + \Theta\, P_\Theta(\lambda+i) \tag{40}$$

In multiblade coordinates Eq. (26) then becomes, considering Eq. (30)

$$\begin{bmatrix} P_{MR}(\lambda) & P_{MI}(\lambda) \\ -P_{MI}(\lambda) & P_{MR}(\lambda) \end{bmatrix} \begin{bmatrix} M_I \\ M_{II} \end{bmatrix} = \begin{bmatrix} P_{\alpha R}(\lambda) & P_{\alpha I}(\lambda) \\ -P_{\alpha I}(\lambda) & P_{\alpha R}(\lambda) \end{bmatrix} \begin{bmatrix} \alpha_I \\ \alpha_{II} \end{bmatrix}$$

$$+ \begin{bmatrix} -P_{\Theta I}(\lambda) & P_{\Theta R}(\lambda) \\ -P_{\Theta R}(\lambda) & -P_{\Theta I}(\lambda) \end{bmatrix} \begin{bmatrix} \Theta_I \\ \Theta_{II} \end{bmatrix} \tag{41}$$

From Fig. 2 there is a cyclic pitch feedback represented by the relation

$$\Theta_I = \alpha_I \,, \quad \Theta_{II} = \alpha_{II} \tag{42}$$

Inserting Eq. (42) into Eq. (41) one then obtains the relations between the rotor moments and the hub angular deflections, from which either rotor receptance or rotor impedance can be computed. The characteristic equation for the rotor alone is obtained by setting $M_I = M_{II} = 0$. Including the feedback from Eq. (42) the characteristic equation reads

$$\begin{vmatrix} P_{\alpha R} & P_{\alpha I} \\ -P_{\alpha I} & P_{\alpha R} \end{vmatrix} + \begin{vmatrix} -P_{\Theta I} & P_{\Theta R} \\ -P_{\Theta R} & -P_{\Theta I} \end{vmatrix} = 0 \qquad (43)$$

This completes step 3 of the analysis.

Impedance or Receptance Matching

It now only remains to match the rotor support to the rotor. The moments transferred from the rotor to the support are

$$(b/2)\,\rho_o\,R^3\,M_I \quad , \quad (b/2)\,\rho_o\,R^3\,M_{II} \qquad (44)$$

whereby the number of blades per rotor, b, must be at least 3, see reference 6. The factor $\rho_o R^3$ is required to obtain dimensional moments. The time unit is still $1/\Omega$, otherwise the expressions (44) would also have to be multiplied by Ω^2. For uniform blades

$$\rho_o\,R^3 = 3\,I_b \qquad (45)$$

and the rotor support dynamic equations without support damping are

$$\begin{bmatrix} \omega_I^2 - \lambda^2 & 0 \\ 0 & \omega_{II}^2 - \lambda^2 \end{bmatrix} \begin{bmatrix} \alpha_I \\ \alpha_{II} \end{bmatrix} = (3\,b/2)(I_b/I) \begin{bmatrix} M_I \\ M_{II} \end{bmatrix} \qquad (46)$$

We can now either insert α_I, α_{II} from Eq. (46) into Eq. (41) (receptance matching) to obtain with Eq. (42) a set of homogeneous equations for M_I, M_{II}. The coefficient determinant then represents the characteristic polynomial. We can also insert M_I, M_{II} from Eq. (46) into Eq. (41)

(impedance matching) and then obtain with Eq. (42) a set of homogeneous equations for α_I, α_{II}.

$$\begin{bmatrix} Q_{11} & Q_{12} \\ Q_{21} & Q_{22} \end{bmatrix} \begin{bmatrix} \alpha_I \\ \alpha_{II} \end{bmatrix} = 0 \tag{47}$$

The total system characteristic equation is then given by

$$\begin{vmatrix} Q_{11} & Q_{12} \\ Q_{21} & Q_{22} \end{vmatrix} = 0 \tag{48}$$

The mode shapes can be easily computed by inserting into Eq. (47) one of the eigenvalues obtained from Eq. (48). One then finds that all modes are either regressing or progressing in the non-rotating reference system. This completes step 4 of the analysis.

If each blade is represented by N point masses, the characteristic equation (48) will be of $4N + 4$ order. For an airframe the receptance or impedance matrix at the rotor-airframe interface will be less simple than Eq. (46). If the airframe is represented by L masses or moments of inertia, the order of the system characteristic equation will be $4N + 2L$. A method to reduce this order without appreciable loss in accuracy of the lower eigenvalues will be discussed later. First some numerical results of solving for the roots of Eq. (48) will be presented.

Numerical Examples

The computations were performed on the IBM-360/65 computer using double precision (16 digits). Single blade computations were made for 5, 8, 10, 15 and 20 elements per blade. The number of 20 elements was found to be too high for the 16 digit precision used. With 10 blade elements no computational difficulties were encountered for the multiblade analysis, provided that the evaluation of the 3 by 3 determinant in Eq. (26) was numerically optimized by writing

$$|\cdots| = -\phi_{33}(\phi_{24}\,\phi_{45} - \phi_{44}\,\phi_{25}) + \phi_{34}(\phi_{23}\,\phi_{45} - \phi_{43}\,\phi_{25}) - \phi_{35}(\phi_{23}\,\phi_{44} - \phi_{43}\,\phi_{24}) \tag{49}$$

whereby the set $\phi_{33}, \phi_{34}, \phi_{35}$ represents the column with the highest values of the elements. A convenient check for adequate computer precision consists of looking at the coefficients of $\lambda^{n_{max}}$, $\lambda^{n_{max+1}}$, etc., in P_θ, whereby n_{max} is the highest power that should occur theoretically in this polynomial. For a single blade with N point masses $n_{max} = 2\,n-2$ for P_θ. If the computer precision is adequate, the coefficients of $\lambda^{n_{max+1}}$, $\lambda^{n_{max+2}}$ are several orders smaller than those of $\lambda^{n_{max}}$. The accuracy of the computation depended on how this determinant was evaluated, see Eq. (49).

Once the single blade problem could be solved without difficulties, the complete coupled system solution posed no further obstacles. The computer accuracy depends on the highest eigenvalue considered and does not suffer when the number of eigenvalues is approximately doubled as for

the coupled system, as long as the highest eigenvalue remains approximately the same. Though 10 point masses per blade would have been satisfactory, the parametric studies for which selected results will be presented here were made with 8 masses per blade. The errors in the first 3 blade eigenvalues shown here were found to be less than one to two percent. For 5 blade elements more substantial eigenvalue errors occur. For 8 masses per blade the equivalent CPU time to obtain a complete set of eigenvalues for the coupled system was 4 seconds, for 55 cases computed in one run the CPU time was 34 seconds.

Single Blade

The two parameters that determine the eigenvalues for the uniform single blade are the non-dimensional bending stiffness q and the Lock number γ. As mentioned before, the rotor speed parameter $q^{-1/2} = 18$ is selected to match the flap-bending frequencies of actual hingeless rotors. For the blade Lock number we select the values $\gamma = 5$ and $\gamma = 8$ that also cover the range of actual hingeless rotors. Though computed for a single blade with Eqs. (27) and (29), we give in Table 1 the eigenvalues in multiblade form to facilitate the comparison with the coupled system eigenvalues to be determined later. The letters R and P refer to regressing and progressing modes respectively. The numbers 1, 2, 3 refer to first, second, third blade flap-bending mode. ξ and ω are real and imaginary part respectively of an eigenvalue.

Table 1

Uncoupled Blade Eigenvalues in Non-Rotating Reference System, $q^{-1/2} = 18$

Flap-Bending Mode	Hinged Blade				Cantilever Blade			
	$\gamma = 5$		$\gamma = 8$		$\gamma = 5$		$\gamma = 8$	
	ξ	ω	ξ	ω	ξ	ω	ξ	ω
1R		.05		.13		.01		.07
	-.311		-.501		-320		-.514	
1P		1.95		1.87		2.01		1.93
2R		1.57		1.55		1.74		1.72
	-.257		-.409		-.265		-.424	
2P		3.57		3.55		3.74		3.72
3R		3.80		3.79		4.17		4.16
	-.229		-.366		-.237		-.378	
3P		5.80		5.79		6.17		6.16

It is seen that there is little difference between the eigenvalues for the hinged and cantilever blade. This is due to the relatively low flap-bending stiffness of the blade as expressed in $q^{-1/2} = 18$. The first natural frequency without aerodynamic damping is 1 for the hinged blade and 1.06 for the cantilever blade. The aerodynamic damping has the effect of lowering the natural frequency. The effect of increasing the Lock number from $\gamma = 5$ to $\gamma = 8$ is merely to increase the damping of each mode in the ratio of 8/5 and to lower the natural frequencies somewhat. The numerical examples for the coupled system will be limited to $\gamma = 5$. When determining the mode shape one finds substantial phase shifts along the blade. For example with $\gamma = 5$ the

first mode of a hinged blade shows between root slope and tip slope a phase shift of 12 degrees. For $\gamma = 8$ the phase shift is still higher. Thus there is a substantial difference between the structural mode shape and the aeroelastic mode shape.

Rotor Alone (Inter Blade Coupling)

Coupling the blades to each other and assuming zero moments at the rotor center, the evaluation of Eq. (43) for $q^{-1/2} = 18$ and $\gamma = 5$ yields the following eigenvalues, whereby the character of a mode as regressing (R) or progressing (P) can be determined from Eq. (47).

Table 2

Rotor Alone Eigenvalues for $q^{-1/2} = 18$, $\gamma = 5$

Flap-Bending Mode	ξ	ω
1R	0	0
1P	-.616	1.96
2R	-.327	1.57
2P	-.193	3.62
3R	-.240	3.87
3P	-.214	5.87

The values of Table 2 should be compared to the values in Table 1 for the hinged blade and $\gamma = 5$. The frequencies are almost the same, and the sum of regressing and progressing mode damping are also the same. However now the regressing and progressing modes have different damping.

With respect to the first regressing mode the frequency and damping are now zero, the damping of the progressing mode is doubled. With respect to the second and third mode the progressing mode damping is reduced, the regressing mode damping is increased.

Unrestrained Rigid Body

When omitting the restraining springs shown in Fig. 1 and the gravitational effect, so that the rotor is coupled to an inertia, one obtains an approximation to the short period pitch and roll modes in helicopter hovering flight mechanics. In Eq. (46) we have $\omega_I = \omega_{II} = 0$. We present here a case of a rotor with 4 blades (b = 4), and an inertia ratio $I_b/I = .2$. Eq. (46) could of course easily be written for different body inertia in pitch and roll. For $q^{-1/2} = 18$, $\gamma = 5$ one obtains:

Table 3

Coupled Rotor-Rigid Body Eigenvalues

$q^{-1/2} = 18$, $\gamma = 5$, $b = 4$, $I_b/I = .2$, $\omega_I = \omega_{II} = 0$

MODE		ξ	ω
Predominant Body	R	-.157	.16
	P	-.167	.16
Predominant Flap-Bending	1R	0	0
	1P	-.316	2.01
	2R	-.265	1.74
	2P		3.74
	3R	-.237	4.17
	3P		6.17

The coupling with a rigid body has added two modes and has substantially changed the rotor alone modes of Table 2. The progressing rotor mode with first flap-bending has only one half the damping. There are now two predominant body modes, one regressing, the other progressing, both with about the same frequency. The second and third flap-bending modes have not been much changed by the coupling with the rigid body.

Rotor and Support Coupling

In evaluating Eq. (46) for a case of a rotor coupled to its support, we assume again 4 blades (b = 4), and now stipulate $I_b/I = 5$. The support frequencies without rotor will be varied from $\omega_I = \omega_{II} = .4$ to 5.5. The frequencies in pitch and roll will first be assumed equal, followed by a case of unequal support frequencies. Table 4 shows the coupled rotor and support eigenvalues for a number of support frequencies $\omega_I = \omega_{II}$. Figure 4 shows the imaginary parts of the eigenvalues, ω, Fig. 5 shows their real parts, ξ. At low support frequencies up to $\omega_I = \omega_{II} < .8$ one can clearly identify a mode as predominantly support or rotor mode. The same is true for high values of $\omega_I = \omega_{II} > 2.5$. In between there is strong coupling between support and rotor, and no predominance can be established. There is an essentially aperiodic mode with very low frequency. It's almost aperiodic decay is quite low for small ω_I, but increases to -.30 at high ω_I. The first progressing rotor flap-bending mode with an uncoupled frequency 1.96 (Table 2) and a high damping increases its frequency and loses its damping with stiffer support. This mode becomes unstable at $\omega_I = \omega_{II} = 1.5$ and only

Table 4

Coupled Rotor and Support Eigenvalues

$q^{-1/2} = 18$, $\gamma = 5$, $b = 4$, $I_b/I = 5$

$\omega_I = \omega_{II}$		.4		.8		1.2		1.6	
MODE		ξ	ω	ξ	ω	ξ	ω	ξ	ω
Support → Rotor 2	R	-.181	1.08	-.168	1.24	-.188	1.44	-.235	1.58
Support → Rotor 1	P	-.310	1.19	-.301	1.37	-.339	1.60	-.403	1.77
Rotor 1	R	-.037	.001	-.109	0	-.172	.002	-.216	.004
Rotor 1 → Support	P	-.176	2.02	-.145	2.03	-.071	2.06	+.019	2.19
Rotor 2 → Support	R	-.206	1.85	-.188	1.87	-.141	1.94	-.077	2.10
Rotor 2	P	-.269	3.76	-.269	3.76	-.269	3.76	-.269	3.76
Rotor 3	R	-.232	4.21	-.232	4.21	-.232	4.21	-.231	4.21
Rotor 3	P	-.237	6.19	-.237	6.19	-.237	6.19	-.236	6.19

$\omega_I = \omega_{II}$		2.5		3.5		4.5		5.5	
MODE		ξ	ω	ξ	ω	ξ	ω	ξ	ω
Support → Rotor 2	R	-.268	1.69	-.269	1.72	-.268	1.73	-.268	1.73
Support → Rotor 1	P	-.398	1.96	-.357	2.00	-.341	2.01	-.333	2.01
Rotor 1	R	-.267	.008	-.290	.011	-.301	.012	-.307	.013
Rotor 1 → Support	P	+.042	2.77	-.053	3.60	-.012	4.65	-.024	5.56
Rotor 2 → Support	R	-.028	2.76	-.049	3.60	-.037	4.74	-.013	5.63
Rotor 2	P	-.267	3.77	-.199	3.83	-.251	3.72	-.261	3.73
Rotor 3	R	-.226	4.22	-.197	4.28	-.206	4.07	-.232	4.13
Rotor 3	P	-.236	6.19	-.236	6.19	-.233	6.20	-.216	6.24

stabilizes again at $\omega_I = \omega_{II} = 3.0$, where it has become a predominant support mode. The second regressing rotor flap bending mode with an uncoupled frequency of 1.57 (Table 2) and a high damping follows essentially the same trend, however without becoming actually unstable. The progressing second flap-bending mode with an uncoupled frequency of 3.6 (Table 2) and a damping of -.19 increases frequency and damping due to coupling with the support. The third flap-bending modes are not much affected by the coupling and correspond to the cantilever cases of Table 1. The change in type of mode when increasing support stiffness is indicated in Table 4 by an arrow. For example Support → Rotor 2 means that for low $\omega_I = \omega_{II}$ we have predominantly a support mode, at high $\omega_I = \omega_{II}$ we have predominantly a second flap-bending rotor mode, both regressing.

The question has often been raised whether airframe modes can be damped by coupling with the rotor. Fig. 5 shows for our case that the support damping from the rotor is very small for support frequencies above 4.5, and that one must avoid support frequencies between 1.5 and 3.0 where a coupled mode is unstable. However for low support natural frequencies below 1.2 the rotor provides very good damping to the support. Obviously the result of Fig. 5 cannot be generalized, since it pertains only to the selected combinations of rotor and support parameters.

In some studies, it was found that unequal stiffness of the rotor support in pitch and roll can alleviate instabilities. In the case of $\omega_I = 1.6$, $\omega_{II} = 4.8$, the following eigenvalues were obtained.

Table 5

Coupled Rotor and Support Eigenvalues

$q^{-1/2} = 18,\ \gamma = 5,\ b = 4,\ I_b/I = 5,\ \omega_I = 1.6,\ \omega_{II} = 4.8$

Mode		ξ	ω
Support	R	-.266	1.63
	P	-.018	4.96
	R	-.216, -.303	0
	P	-.357	1.90
Rotor 2	R	-.027	2.15
	P	-.262	3.74
Rotor 3	R	-.226	4.16
	P	-.234	6.20

As compared to the case of $\omega_I = \omega_{II} = 1.6$ in Table 4 the instability is removed, though the second regressing rotor mode has now almost no damping.

Reducing the Order of the Characteristic Equation

Although for the simple case assumed her there was no difficulty in solving the characteristic equation, the introduction of more degrees of freedom for the blades (in-plane bending and torsion) and of a much higher order for the airframe receptance or impedance polynomials may lead to difficulties. It has been suggested in reference 7 to reduce the order of the characteristic equation of coupled large systems by modalizing and truncating the component receptance matrices. It is, therefore, of interest to find out

whether the method suggested in reference 7 can result in a lower order characteristic equation without an appreciable reduction in accuracy for the lower eigenvalues. Let us write Eq. (26) in the form

$$M_{N+1}\, P_M(\lambda)/P_\alpha(\lambda) = y'_{N+1} + \theta\, P_\theta(\lambda)/P_\alpha(\lambda) \tag{50}$$

We now determine the roots of

$$P_\alpha(\lambda) = 0 \tag{51}$$

which according to Eq. (27) are the eigenvalues for the single blade that is hinged at the root and experiences no feedback from pitch angle θ. We then perform a partial fraction expansion of the two polynomials $P_M(\lambda)/P_\alpha(\lambda)$ and $P_\theta(\lambda)/P_\alpha(\lambda)$ with respect to the roots of Eq. (51). Since the roots occur in conjugate complex pairs, we have for example

$$P_M(\lambda)/P_\alpha(\lambda) = C_o + \frac{C_1}{\lambda - \lambda_1} + \frac{C_1^*}{\lambda - \lambda_1^*} + \cdots \tag{52}$$

and a similar expression for $P_\theta(\lambda)/P_\alpha(\lambda)$. This partial fraction expansion is now truncated, and Eq. (26) is rewritten as

$$M_{N+1}\, \overline{P}_M(\lambda) = y'_{N+1}\, \overline{P}_\alpha(\lambda) + \theta\, \overline{P}_\theta(\lambda) \tag{53}$$

where the new polynomials $\overline{P}_M(\lambda)$, $\overline{P}_\alpha(\lambda)$, $\overline{P}_\theta(\lambda)$ are of lower order than the original polynomials. From here on the analysis follows the same procedure as described before leading to the total system characteristic equation (48) which now is of lower order.

Using the case $\omega_I = \omega_{II} = 1.2$ in Table 4 and omitting in Eq. (52) the last 8 terms, one obtains the following total system eigenvalues.

Table 5

Coupled Rotor and Support Eigenvalues
with Truncated Polynomials

$q^{-1/2} = 18$, $\gamma = 5$, $b = 4$, $I_b/I = 5$, $\omega_I = \omega_{II} = 1.2$

MODE		ξ	ω
Support → Rotor 2	R	-.200	1.44
Support → Rotor 1	P	-.384	1.62
Rotor 1	R	-.158	.008
Rotor 1 → Support	P	-.038	2.11
Rotor 2 → Support	R	-.139	2.04
Rotor 2	P	**-.271**	3.80
Rotor 3	R	-.232	4.34
	P	-.239	6.31

In comparing these numbers with those in Table 4 for $\omega_I = \omega_{II} = 1.2$ it is seen that the truncation method has resulted in good approximations. It can be shown that these approximations are better than those obtained from performing the eigenvalue analysis with only 4 blade elements. Furthermore reference 7 suggests an iteration method to improve the accuracy of any specific eigenvalue, that was found to rapidly converge to the exact value in a numerical example. From Table 5 there seems to be no doubt that for the rotor-airframe coupling problem modalization of the polynomials with the single hinged blade eigenvalues and subsequent truncation of the partial fraction expansion is a viable method to reduce the order of the total system characteristic equation, if this is required.

Concluding Remarks

In the conventional stability analysis for coupled rotor-airframe systems structural modes are used where all parts of the system oscillate in phase. In order to approximate the actual modes, where due to aerodynamic effects substantial phase differences exist between the oscillations of the various parts of the system, several structural modes must be superimposed, and it is difficult to judge how many of the structural modes are needed to properly represent a true aeroelastic mode. In the finite element stability analysis explored here for the case of coupled blade flap-bending and airframe oscillations the aerodynamic effects are directly incorporated into the blade element transfer matrices. The resulting natural modes are true aeroelastic modes and the problem of structural mode superposition is eliminated. Computational limitations occur due to numerical errors from repeated multiplications of high order polynomials. For 10 blade elements and performing the computations with 16 digits the numerical errors present no problem. The analysed system is then of 44th order. Though the method should be tried out on more sophisticated descriptions of both the rotor and the airframe to include blade chordwise bending and blade torsion and a more complex airframe structure, it appears from the experience gained so far, that the principal limitation is in the largest eigenvalue considered. It can be anticipated that with more eigenvalues but approximately retaining the largest one, no numerical difficulties will be encountered, except that the order of the characteristic equation may become too high for accurate root extraction. In this case the method of modalizing and truncating the polynomials, briefly studied herein, could be applied to reduce the order of the total system characteristic equation.

While the main purpose of this investigation was to shed some light on the tractability of the finite element stability analysis for coupled rotor-airframe systems, interesting results were obtained in the numerical examples. For the selected ratio of blade flapping moment of inertia over rotor support inertia of 5, and for the selected hingeless blade first natural flap-bending frequency without damping and while rotating of 1.06 there are 4 strongly coupled aeroelastic modes, 2 modes that are for small and for large support stiffness mainly support modes, and 2 further modes that are in these regions mainly progressing first blade-flap bending and regressing second blade-flap bending modes. Two of these modes can become unstable or near unstable in the intermediate range of support stiffness. The progressing second blade flap bending and the higher blade bending modes show little tendency of coupling with the rotor support and retain high damping. The extension of the finite element stability analysis to forward flight conditions should pose no great difficulties as long as the rotor advance ratio is moderate and constant coefficients in the multiblade equations can be considered adequate.

References

1. Isakson, G. and Eisley, J. G., "Natural Frequencies in Bending of Twisted Rotating and Nonrotating Blades". NASA TN D-371, March 1960.

2. Isakson, G. and Eisley, J. G., "Natural Frequencies in Coupled Bending and Torsion of Twisted Rotating and Non-rotating Blades", NASA CR-65, July 1964.

3. Curtiss, H. C., Jr. and Shupe, N. K., "A Stability and Control Theory for Hingeless Rotors", 27th Annual National Forum, American Helicopter Soc., Washington, D.C., May 1971, Preprint 541.

4. Bielawa, R. L., "Blade Stress Calculations - Mode Deflection vs. Force Integration", AHS Mideast Region Symposium on Rotor Technology, August 1976.

5. Johnston, R. A., "Rotor Stability Prediction and Correlation with Model and Full-Scale Tests", Journal American Helicopter Soc., Vol. 21, No. 2, April 1976, pp. 20-30

6. Hohenemser, K. H. and Yin, S. K., "Some Applications of the Method of Multiblade Coordinates", Journal American Helicopter Society, Vol. 17, No. 3, July 1972, pp. 3-12.

7. Kung, Wei-chi and Hohenemser, K. H., "Eigenvalue Analysis for Coupled Large Linear Damped Structures", Computer Methods in Applied Mechanics and Engineering, 1977.

Figure Captions

Fig. 1 Schematic of Rotor and Support System

Fig. 2 Angular Deflection in Pitch of Hub Relative to Reference System

Fig. 3 Blade Element in Flap-Bending

Fig. 4 Frequencies of Aeroelastic Coupled Modes for the Case of Table 4

Fig. 5 Damping of Aeroelastic Coupled Modes for the Case of Table 4

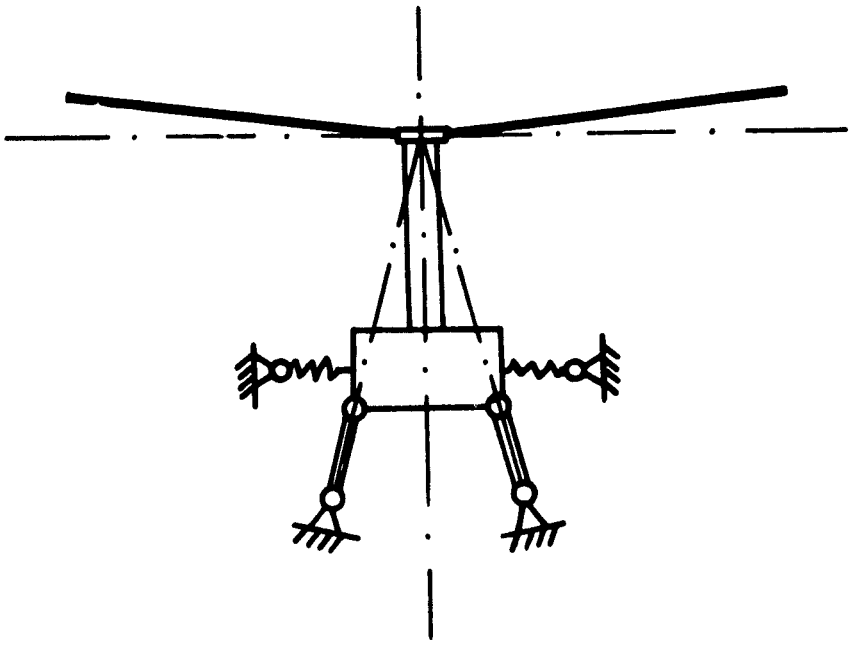

Fig. 1

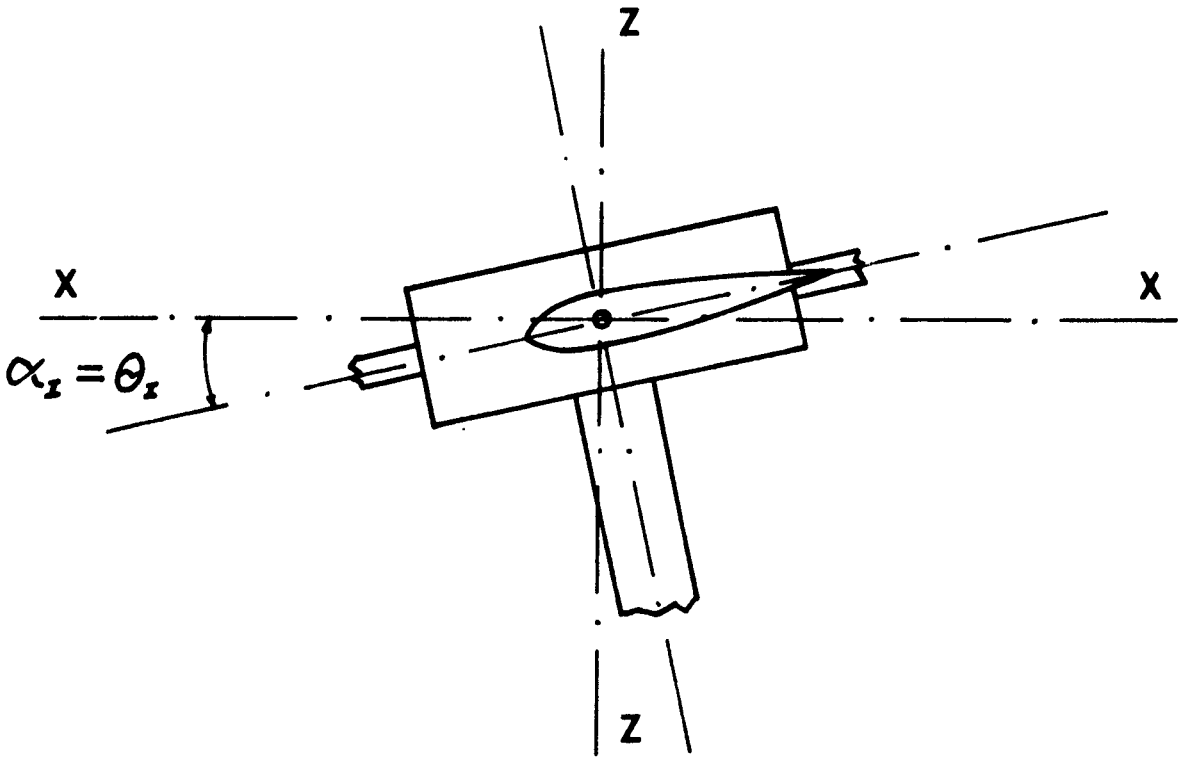

Fig. 2

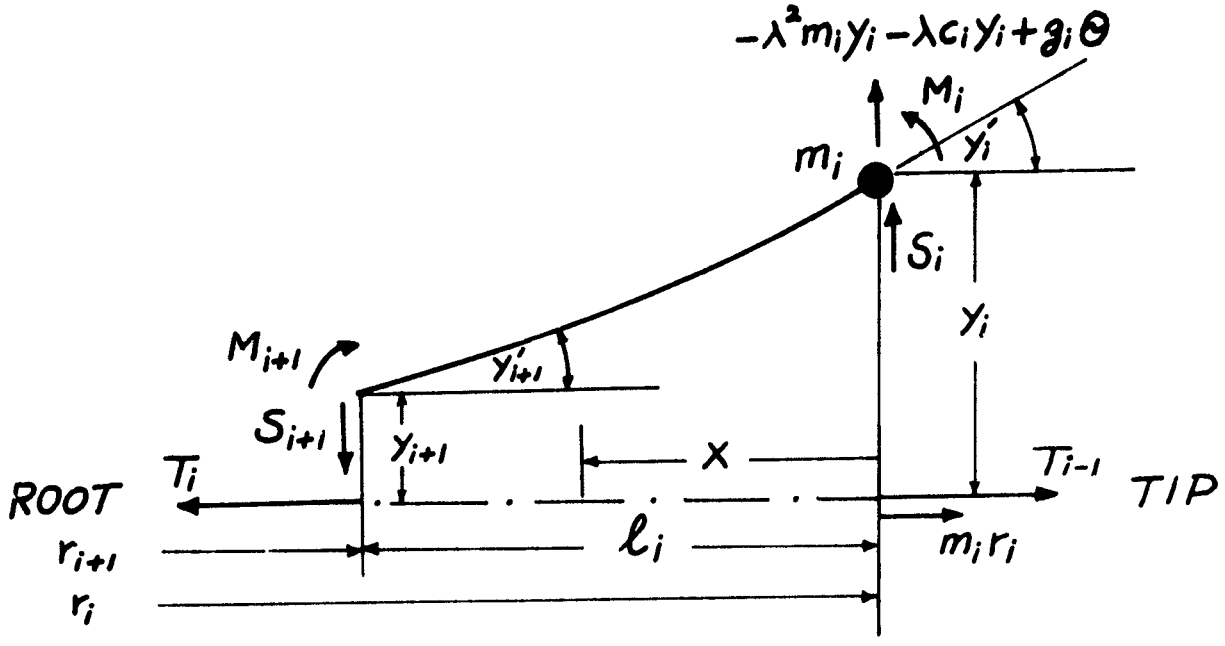
$-\lambda^2 m_i y_i - \lambda c_i y_i + g_i \Theta$
M_i
m_i
y_i'
S_i
y_i
M_{i+1}
y_{i+1}'
S_{i+1}
y_{i+1}
x
T_i
T_{i-1}
ROOT
TIP
r_{i+1}
ℓ_i
$m_i r_i$
r_i

Fig. 3

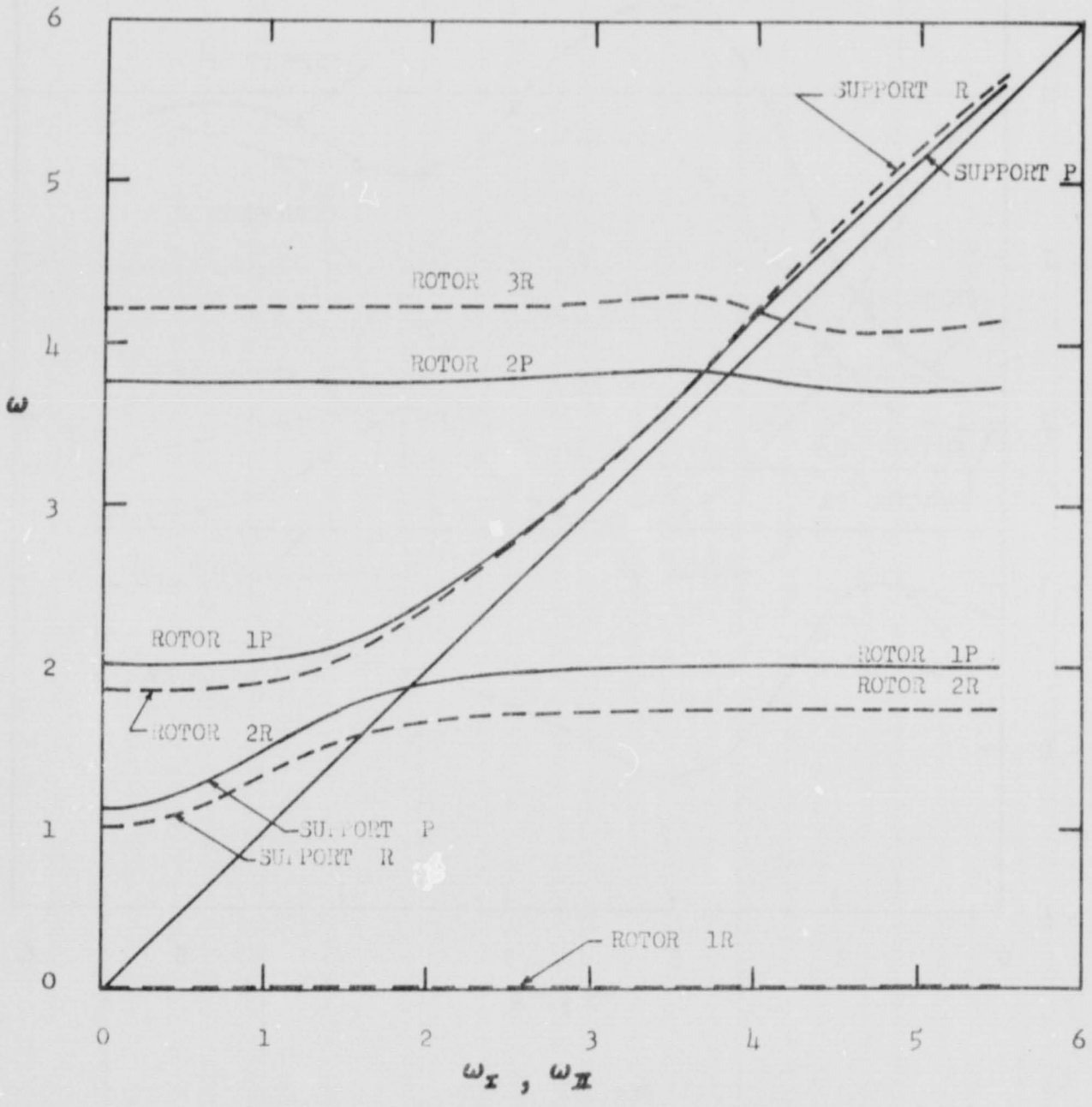
6
5
4
3
2
1
0
ω
0
1
2
3
4
5
6
ω_I , ω_{II}
SUPPORT R
SUPPORT P
ROTOR 3R
ROTOR 2P
ROTOR 1P
ROTOR 1P
ROTOR 2R
ROTOR 2R
SUPPORT P
SUPPORT R
ROTOR 1R

Fig. 4

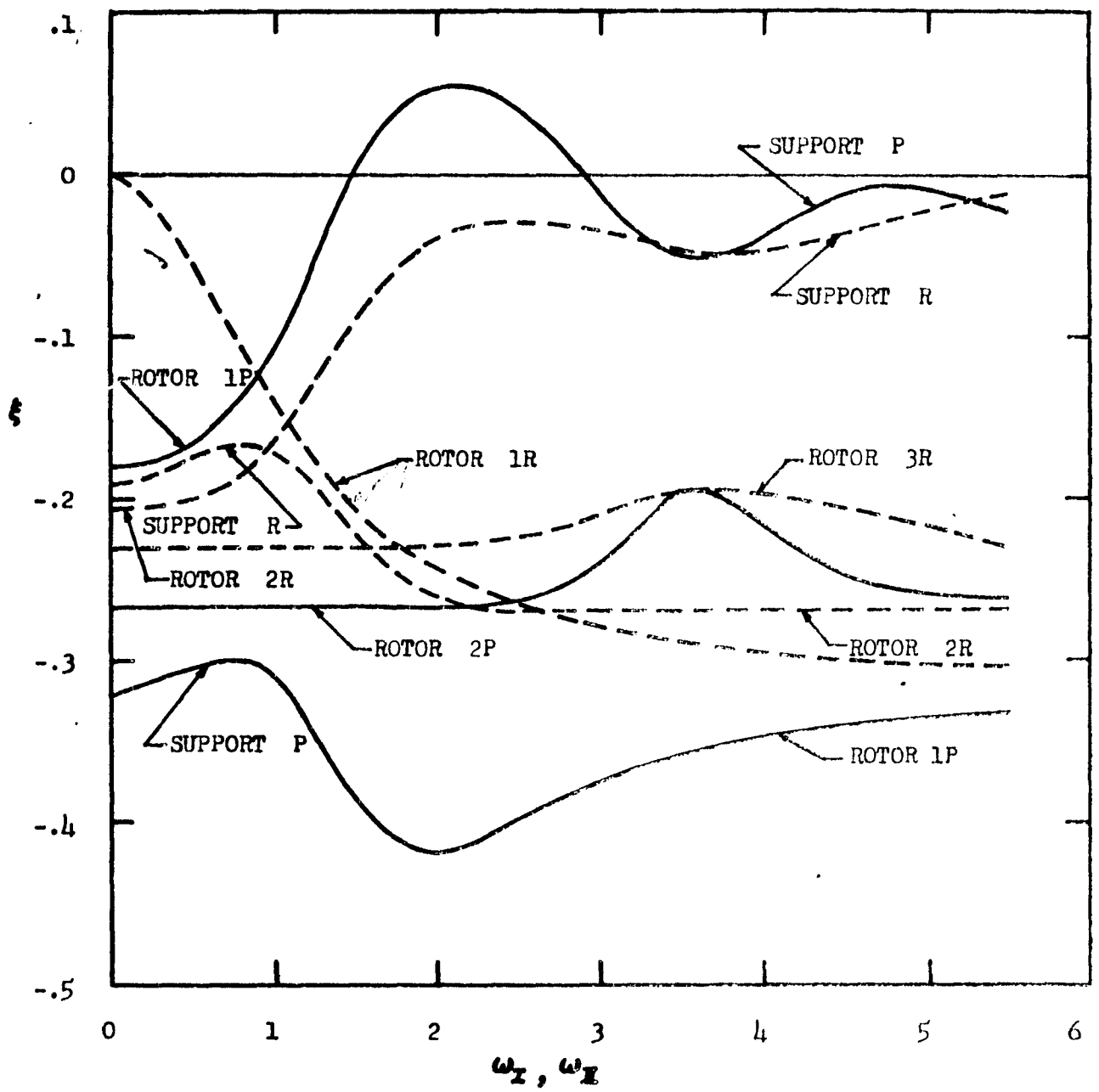
.1
0
-.1
-.2
-.3
-.4
-.5
ξ
0
1
2
3
4
5
6
ω_I , ω_{II}
SUPPORT P
SUPPORT R
ROTOR 1P
ROTOR 1R
ROTOR 3R
SUPPORT R
ROTOR 2R
ROTOR 2P
ROTOR 2R
SUPPORT P
ROTOR 1P

Fig. 5